WARSAW UNIVERSITY OF TECHNOLOGY Index 351733
FACULTY OF CIVIL ENGINEERING
COMMITTEE FOR CIVIL AND WATER ENGINEERING
POLISH ACADEMY OF SCIENCES ISSN 1230-2945
DOI: 10.24425/ace.2023.144174
ARCHIVES OF CIVIL ENGINEERING
Vol. LXIX ISSUE 1 2023
pp. 287 –306

Research paper

Seismic performance of horizontal swivel system of asymmetric continuous girder bridge

Jiawei Wang[1], Hongshuai Gao[2], Kexin Zhang[3], Zongyun Mo[4], Hongchun Wang[5]

Abstract: The bridge horizontal swivel system generally adopts a symmetrical structure and uses a spherical hinge structure that can adjust the rotation to complete rotation construction. Because of the complexity of railway lines under bridges, some asymmetrical horizontal swivel systems have been increasingly applied in practical engineering in recent years. This system is more suitable for areas with complex railway lines, reduces the bridge span, and provides better economic benefits. However, it is also extremely unstable. In addition, instability can easily occur under dynamic loads, such as earthquake action and pulsating wind effects. Therefore, it is necessary to study their mechanical behavior. Based on the horizontal swivel system of an 11,000-ton asymmetric continuous girder bridge, the dynamic response of the horizontal swivel system to seismic action was studied using the finite element simulation analysis method. Furthermore, using the Peer database, seismic waves that meet the calculation requirements are screened for time-history analysis and compared to the response spectrum method. The mechanical properties of the structural system during and after rotation were obtained through calculations. During rotation, the seismic response of the structure is greater. To reduce the calculation time cost, an optimization algorithm based on the mode shape superposition method is proposed. The calculation result is 87% that of the time-history analysis, indicating a relatively high calculation accuracy.

Keywords: asymmetric continuous beam, simulation analysis of rotation process, time history analysis method, rotation construction method

[1]PhD., Eng., Anhui Polytechnic University, School of Architecture and Civil Engineering, Wuhu City, Beijing Middle Road, China, e-mail: wjw526@126.com, ORCID: 0000-0002-1263-3150
[2]PhD., Eng., Heilongjiang University, College of Civil Engineering, Harbin City, Xuefu Road, China, e-mail: ghsphd@126.com, ORCID: 0000-0002-9304-5966
[3]PhD., Eng., Shenyang Jianzhu University, School of Architecture and Civil Engineering, Shenyang City, Hun Nan Road, China, e-mail: jt_zkx@sjzu.edu.cn, ORCID: 0000-0001-6610-0045
[4]PhD., Eng., Anhui Polytechnic University, School of Architecture and Civil Engineering, Wuhu City, Beijing Middle Road, China, e-mail: mozongyun2004@163.com, ORCID: 0000-0002-6308-5967
[5]Eng., Anhui Polytechnic University, School of Architecture and Civil Engineering, Wuhu City, Beijing Middle Road, China, e-mail: 3438673085@qq.com, ORCID: 0000-0003-0895-4899

1. Introduction

Previous studies have shown that conventional construction methods are unsuitable for constructing continuous girder bridges that cross railways. For example, during the construction of the support structure, the normal passage of the railway under the bridge is affected, and constructing hanging baskets must be segmental and symmetrical, which is time-consuming, causes traffic under the bridge, and poses security risks. In contrast, the swivel construction method is generally parallel to the railway line. After completing the construction of the superstructure, swivel piers and hinges are rotated by an angle along the central axis through horizontal traction equipment [1–5]. The swivel construction of the bridge is thus finally completed.

The horizontal rotation construction method has developed rapidly worldwide [6, 7]. Bridge swivel weight has increased from thousands to tens of thousands of tons, from counterweight to no counterweight, and from straight bridges to curved bridges [8]. The asymmetrical swivel construction method is currently used in some areas with restricted site conditions. The inconsistency of the spans on both sides of the cantilever causes the structure to exhibit a certain eccentric effect. This type of structure has poor rotational stability and is easily unstable under dynamic loads such as earthquake action and the pulsating wind effect. As a result, further research into the dynamic characteristics of horizontal swivel systems in asymmetric continuous girder bridges is required.

The non-symmetrical continuous beam horizontal swivel system is jointly established by the spherical hinge and support foot structure during the rotation process. However, the structural constraints are weak. Furthermore, different spans on both sides of the structure generate a certain unbalanced moment simultaneously. When a structure is subjected to an earthquake, it becomes unstable. This situation can be avoided by conducting a seismic analysis, optimizing the design for the weak parts, and improving the seismic performance of the structure. Seismic research on horizontal rotation systems mainly focuses on the bridge state, which completes the structural system conversion after the structure is rotated. As a project, He Wei used a T-shaped rigid-frame swivel bridge to calculate the internal force of a structure under the action of an earthquake using the seismic response spectrum method. The horizontal swivel system was found to be in an elastic stress state, and the structural bearing capacity satisfied the design requirements [8]. However, both ends of the T structure were supported, the piers were consolidated, and the seismic response analysis of the maximum cantilever state during the rotation process was not performed because this study is limited to analysis of the complete bridge state. The system was more prone to instability under dynamic loads because of its inadequate restraint in the maximum cantilever state. Even though the earthquake action is a combination of accidental effects, important bridges in earthquake-prone areas or bridges with low stiffness must undergo seismic calculations and isolation design. Generally, bridges constructed using swivel technology are located on important roads and railway intersections. As a result, seismic calculations must be performed on the swivel bridge in both the maximum can-

tilever state (during the swivel process) and the completed bridge state (i.e., the swivel is completed).

In this study, a calculation method for seismic time history analysis of the system in the maximum cantilever state (during the process of rotation) and the bridge state (after the rotation is complete) is studied based on an 11,000-ton asymmetric continuous girder bridge horizontal rotation system. An optimization algorithm for the seismic response of the horizontal swivel system of asymmetric continuous girder bridges was proposed by comparing the mechanical properties of the two states and the reasons for the differences.

2. Research method

2.1. An overview of the bridge

The supporting project is a continuous girder bridge of equal height and an asymmetric structure with a span of 50+60 m.The upper structure of the bridge has a C50 concrete single-box three-chamber prestressed concrete box girder. The width of the bridge deck is 21.3 m, and the cantilevers on both sides of the box girder are 3 m long. The thickness of the end of the cantilever plate is 20 cm, that of the root is 50 cm, that of the top plate of the middle fulcrum box girder is 70 cm, and that of the bottom plate is 190 cm. The height of the beam is 4.5 m, and the swivel weight of the bridge is approximately 11,000 tons. The spherical hinge structure has a concrete spherical hinge structure. To improve the compressive strength of the spherical hinge and the flatness of the contact surface, steel pipe constraints were set on the outside of the concrete spherical hinge and at the position of the spherical surface, with the interior filled with C50 concrete. The dimensions of each part of the horizontal swivel system are shown in Fig. 1.

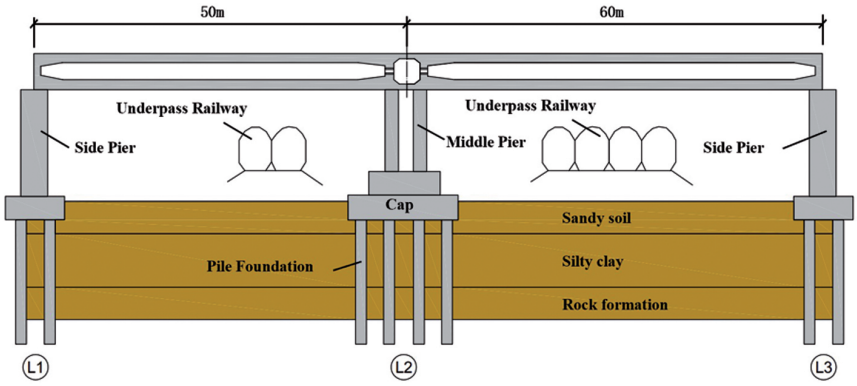

(a) Size of swivel bridge (unit: m)

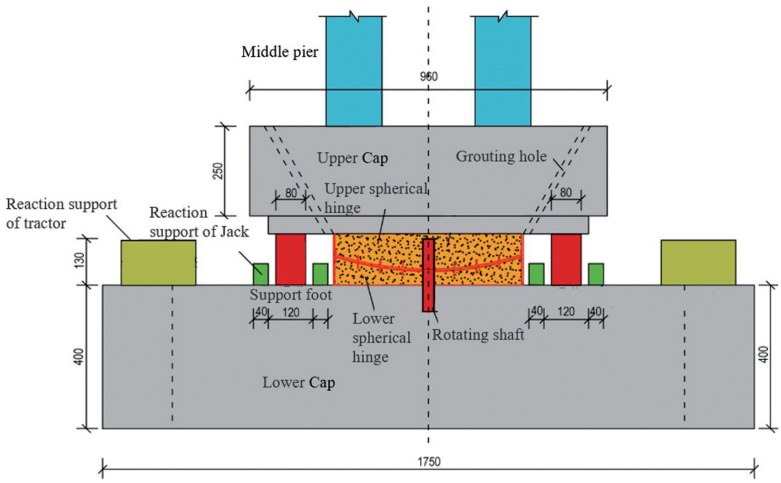

(b) Structure of spherical hinge (unit: cm)

Fig. 1. Dimensions of each part of the horizontal swivel system

2.2. Simulation model

This study used ANSYS-APDL15.0 software for modeling. Two models were developed for this simulation model to study the rotating process of the state of the bridge. Model 1 simulated the rotation process: both sides of the upper structure of the bridge were unconstrained, and the structure was supported by spherical hinges and support feet. The rotational process model is shown in Fig. 2a). As shown in Fig. 2b), Model 2 is a bridge state model in which both sides of the upper structure are connected to the side pier supports and the middle pier is consolidated with the cap.

Because the model adopts the time history analysis method, the majority of the load steps in the seismic wave time history file in each direction exceeded 10,000. To improve the calculation efficiency, a Beam188 element was used in this simulation model to simulate the element with a spatial 3D finite strain structure with two nodes, each node having six degrees (three horizontal and three rotational). The X-axis of the local coordinate system is the line connecting the two nodes of the beam element, and the element could withstand various deformations. The MPC184 element was used to simulate the connection between the pier and the main girder. In the maximum cantilever state of the system, the structure was only constrained by the spherical hinge structure: the vertical force support was provided by the intermediate spherical hinge, and the lateral and longitudinal bending moment supports were provided by several surrounding foot structures. This balanced the entire structure. The position of the pier bottom adopted consolidation treatment. Model 2 considered the influence of side pier constraints on the structure and set the vertical and horizontal constraints on the pier. The bridge deck pavement used a mass of 21 units to set inertia in three directions (x, y and z).

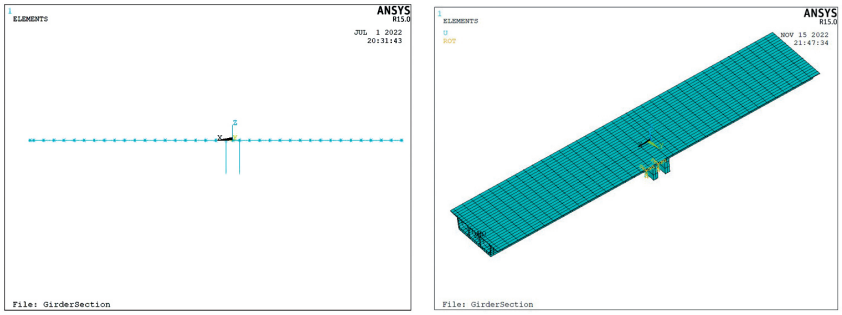

(a) Model 1

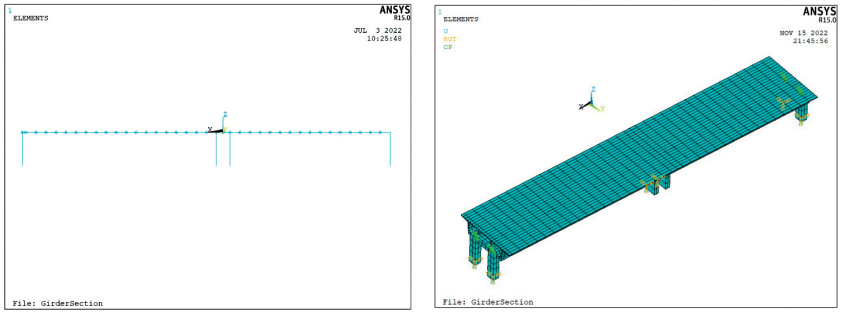

(b) Model 2

Fig. 2. Structural Simulation Model

The definition of damping is important in the dynamic time-history analysis structure. In this study, the damping force is proportional to the structure's speed. When transient analysis is used in the ANSYS solver, structural damping adopts Rayleigh damping, as shown in Eq. (2.1) [9].

$$[C] = \alpha[M] + \beta[K] \tag{2.1}$$

where $[C]$ is the damping matrix, $[M]$ is the mass matrix, $[K]$ is the stiffness matrix, α is the mass damping coefficient, and β is the stiffness matrix coefficient. The relationship between coefficients α and β and the viscosity proportional coefficient ξ is given by Eq. (2.2).

$$\frac{\alpha}{(2 \times \omega)} + \beta \times \frac{\omega}{2} = \xi \tag{2.2}$$

In the above formula, f is the structural frequency, and $\omega = 2\pi f$. The two sets of equations below were obtained through structural modal calculations.

$$\frac{\alpha}{(2 \times \omega 1)} + \beta \times \frac{\omega 1}{2} = \xi$$

$$\frac{\alpha}{(2\times\omega 2)}+\beta\times\frac{\omega 2}{2}=\xi$$

The Eq. (2.3) is obtained by combining the above formulas:

$$\alpha=\frac{4\times\pi\times f_1\times f_2\times\xi}{(f_1+f_2)}$$
$$\beta=\frac{2\times\xi}{(\omega_1+\omega_2)}=\frac{\xi/\pi}{(f_1+f_2)} \tag{2.3}$$

2.3. Structural modal analysis

The structural dynamic properties are affected by the mass distribution and structural boundary conditions. The mode-shape frequencies of the same order in Models 1 and 2 were different. This study used the Lanczos method to calculate the first 10 modes of the structure, and the structural mass participation coefficient was over 95%. The mode frequencies and vibration forms are listed in Table 1.

Table 1. Natural frequencies and modes of the first ten modes of the structure

Model number	Natural frequency/Hz		Mode of vibration	
	Model 1	Model 2	Model 1	Model 2
1	0.411	1.952	The girder and the middle pier bent laterally, the 1st mode	The middle pier bent longitudinally, the 1st mode
2	0.522	2.497	The girder bent longitudinally, the 1st mode	Side pier bent laterally, the 1st mode
3	0.876	3.098	The girder bent longitudinally, the 2nd mode	The girder bent longitudinally, the 1st mode
4	1.891	3.718	The middle pier bent longitudinally, the 1st mode	Side pier bent laterally, the 2nd mode
5	2.241	4.516	The girder bent laterally, the 2nd mode	The girder bent longitudinally, the 2nd mode

Table 1 shows that the middle piers of Models 1 and 2 have the same frequencies of the first-order longitudinal bending mode shapes, which suggests that the side piers have inadequate longitudinal restraints on the main girder and that the internal force and deformation of the piers under the influence of longitudinal loads are also the same.

2.4. Earthquake input

The earthquake's input process was the main influencing factor in the seismic response analysis. In general, the horizontal seismic action of the structure in the two main axis directions must be calculated, while the horizontal seismic action in each direction is

borne by the force-resistant components in that direction. Nonetheless, vertical seismic action cannot be ignored when calculating long cantilever and long-span structures. The seismological calculations consider acceleration in three main directions: transverse bridge, longitudinal bridge, and vertical direction. This simulates the acceleration peak value, spectral characteristics, and earthquake duration of the multi-degree-of-freedom system during earthquakes.

The time-history analysis selected actual strong earthquake records or artificially simulated acceleration time history according to the site category. Simultaneously, the actual seismic records account for at least two-thirds of the total number, and the average value of the shear force at the bottom of the bridge pier calculated by multiple seismic waves accounts for at least 80% of the results calculated by the response spectrum method [10, 11]. The study used seismic waves recorded by actual strong earthquakes to obtain the real response of the continuous rigid frame bridge in the maximum cantilever state, and the maximum value was used as the calculation basis. These strong earthquake records were based on the seismic database of the Pacific Earthquake Engineering Research Center (PEER). Multiple groups of suitable seismic waves were screened out by inputting the design response spectrum and the first three-order natural vibration period of the structure. The actual response spectrum was obtained via the Fourier transform. When the acceleration value under the first-order natural vibration period was compared to the design response spectrum, the difference was less than 30%. The seismic waves were screened based on this principle. The screening results revealed that the seismic records from the same group of ground motions, HMC180, HMC270, and HMCDWN, could not meet the requirements of an error of less than 30% simultaneously under the first-order natural vibration period. Therefore, the seismic waves of Models 1 and 2 in three directions were generated using different seismic data, and six seismic waves that met the requirements were screened out of 50 strong earthquake records. In this study, the comparison data for the time history analysis used the acceleration response spectrum in "Seismic Rules for Highway Bridges" [11] as shown in Eq. (2.4).

$$s = \begin{cases} S_{A\max} \times (5.5T + 0.45) & T < 0.1 \text{ s} \\ S_{A\max} & 0.1 \text{ s} \le T \le T_g \\ S_{A\max} \times (T_g/T) & T > T_g \end{cases} \tag{2.4}$$

where $S_{A\max}$ is the maximum seismic acceleration, T_g is the characteristic period, and T is the natural vibration period.

Real seismic waves were screened via the characteristic period and first three-order natural vibration frequencies of the structure. These two models were studied in six directions. Furthermore, six real seismic waves were screened. Fig. 3 to Fig. 6 show the acceleration time-history curve and seismic wave response spectrum 1 of Models 1 and 2, respectively.

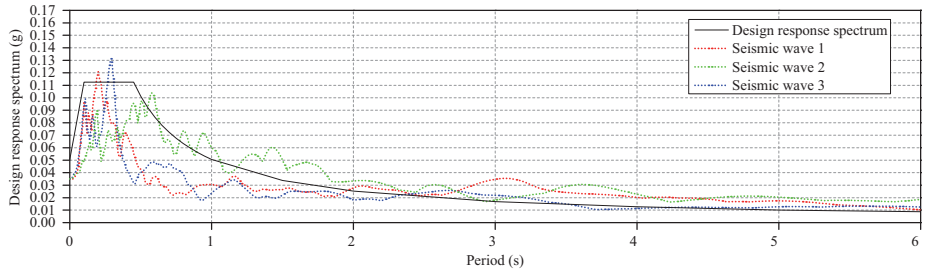

Fig. 3. Model seismic wave calculation response spectrum and design response spectrum comparison

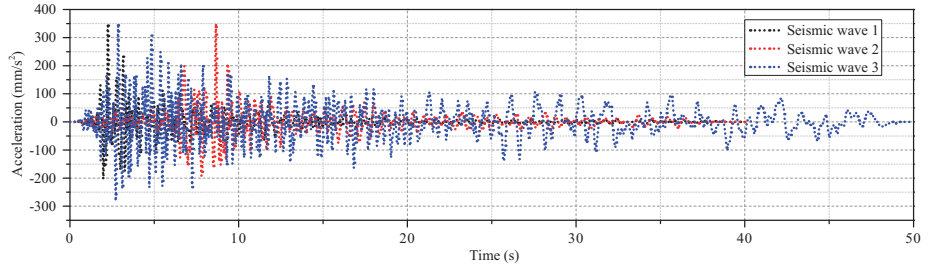

Fig. 4. Time history of three seismic waves in Model 1

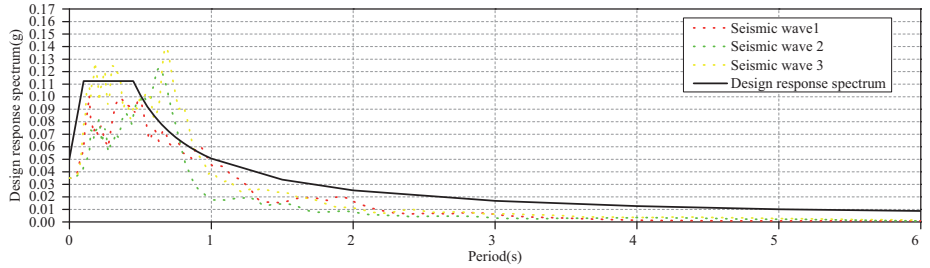

Fig. 5. Comparison of seismic wave calculation response spectrum and design response spectrum in Model 2

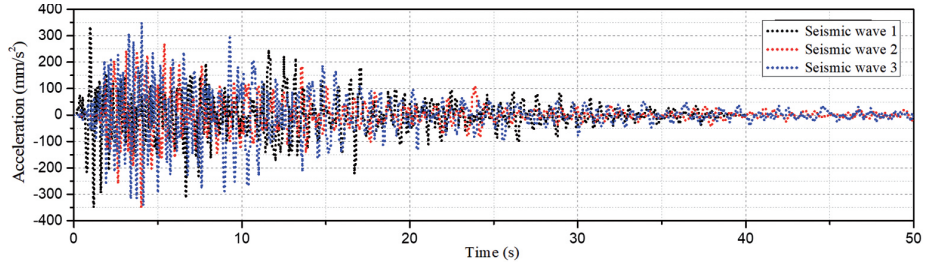

Fig. 6. Time history of three seismic waves in Model 2

3. Results and discussion

3.1. Model calculation results

3.1.1. Seismic Response Analysis of Model 1

The two models were subjected to a nonlinear dynamic time-history analysis, and the results of the time-history analysis were compared to those calculated using the response spectrum method. The time integration function in ANSYS must be considered in the calculation; otherwise, the cumulative effect of seismic action cannot be considered. The time step of the seismic wave was 0.005 s, and the calculation step was consistent with the seismic wave record. The peak values of the internal force response of the maximum cantilever state of the bridge (rotation process model) are listed in Table 2 to Table 4.

Table 2. Transverse seismic response of the bridge (force unit: kN, bending moment unit: kN·m)

Position	Internal force	Seismic Wave 1	Seismic Wave 2	Seismic Wave 3	Maximum value	Average value	Response Spectrum Results
Pier top	shear force *Fy*	1540	1880	2760	2760	2060	2169
	bending moment *Mx*	2007	1277	2013	2013	1766	1477
Pier bottom	shear force *Fy*	1597	1955	2833	2833	2128	2650
	bending moment *Mx*	15758	19746	29296	29296	21600	19629
Cantilever root	shear force *Fy*	1494	1838	2721	2721	2018	1590
	bending moment *Mz*	51297	60192	94791	94791	68760	38200

Table 3. Longitudinal bridge seismic response (force unit: kN, bending moment unit: kN·m)

Position	Internal force	Seismic Wave 1	Seismic Wave 2	Seismic Wave 3	Maximum value	Average value	Response Spectrum Results
Pier top	axial force *Fz*	2334	6623	3028	6623	3995	2311
	shear force *Fx*	1291	2884	4493	4493	2889	2262
	bending moment *My*	6341	14721	22479	22479	14514	10424
Pier bottom	axial force *Fz*	2334	6223	3029	6223	3862	3315
	shear force *Fx*	1306	3009	4638	4638	2984	1967
	bending moment *My*	6758	11951	23447	23447	14052	12223
Cantilever root	bending moment *My*	5736	15134	18318	18318	13063	11486

Table 4. Vertical seismic response (unit of force: kN, unit of bending moment: kN·m

Position	Internal force	Seismic Wave 1	Seismic Wave 2	Seismic Wave 3	Maximum value	Average value	Response Spectrum Results
Pier top	axial force *Fz*	1727	4853	2734	4853	3105	4393
	shear force *Fx*	136	405	205	405	249	88
	bending moment *My*	941	2620	1240	2620	1600	752
Pier bottom	axial force *Fz*	1726	4703	2813	4703	3081	4496
	shear force *Fx*	137	406	206	406	250	151
Pier bottom	bending moment *My*	556	1526	830	1526	971	461
Cantilever root	shear force *Fz*	1173	3535	2021	3535	2243	4086
	bending moment *My*	15989	15252	14492	15252	15244	11353

The following conclusions can be drawn from the data in Table 2 to Table 4:

– First, under transverse seismic input, the main responses of the earthquake are the transverse bending moment of the pier bottom, transverse shear force, and transverse bending moment of the girder. The internal force at the top of the pier was smaller than that at the bottom of the pier. Furthermore, the axial forces at the pier and main girder were very small, and the control parameter was the transverse bending moment at the bottom of the pier. The calculated results for the three seismic waves were relatively discrete, and their average results were close to the calculated results for the response spectrum.
– Second, the main seismic response to the longitudinal seismic input was the longitudinal bending moment of the pier bottom and pier top. Under this condition, the longitudinal bending moment of the bridge pier and the longitudinal bending moment of the cantilever root of the main girder are the control parameters. The calculated results of the three seismic waves were relatively discrete, and their average results were close to those for the response spectrum.
– Third, under the vertical seismic input, the main seismic response is the axial force of the bridge pier and the longitudinal bending moment at the cantilever root of the girder, which exceeds the seismic response in the longitudinal bridge direction. The vertical axial force of the pier and the longitudinal bending moment of the cantilever root of the girder are the control parameters. The average results were close to response spectrum calculation results, as were the results for the three seismic waves.

This study selected the maximum value in the time history analysis as the calculation basis to obtain the most unfavorable result of earthquake action. Based on the above analysis results, the transverse bending moment of the bridge pier was calculated in time-history

analysis using seismic wave 3, the longitudinal bending moment was calculated using seismic wave 3, and the axial force was calculated using seismic wave 2. The transverse and longitudinal bending moments of the main girder were calculated using seismic wave 3. The internal force time history curves of each control section are shown in Fig. 7.

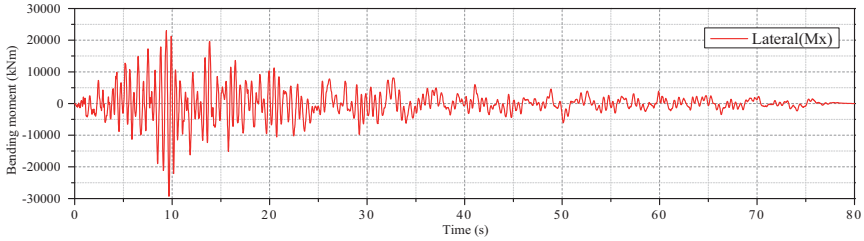

(a) Bending-moment time history (Results of Seismic Wave 3)

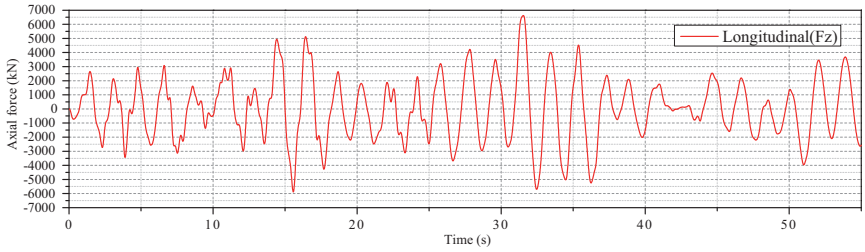

(b) Axial force–time history (Results of Seismic Wave 2)

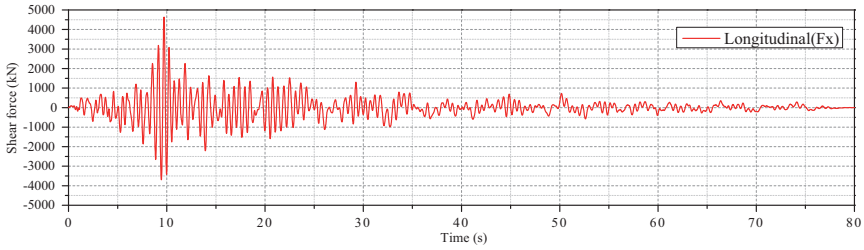

(c) Time History of the shear force (Results of Seismic Wave 3)

Fig. 7. Internal force response of pier bottom

Based on Fig. 7 and Table 2 to Table 4, the following conclusions can be drawn:

– The bending moment value at the top of the pier presents a trend of oscillation and decline, which is consistent with the stress characteristics of the structure under the condition of its own damping. The maximum longitudinal bending moment at the top of the pier reached 22479 kN·m, which occurred at 9.955 s in the initial period of the earthquake. The axial force time-history curve was relatively uniform, with a maximum value of 6623 kN.

– The maximum transverse bending moment of the pier bottom was 29296 kN·m, which appeared at 9.975 s in the initial earthquake period. The time-history curve of the axial force was relatively uniform, with a maximum value of 6223 kN. The bending moment and axial force at the bottom of the pier were larger than those at the top. Furthermore, this section focuses on seismic design. Because the pier top and bottom were calculated using the same waveform, the entire time-history curve obtained was roughly the same. However, the maximum value of the pier top appeared later than that of the pier bottom, indicating that the vertical structure has an impact on the time corresponding to the maximum response of the structure under the same earthquake.
– The main beam's maximum transverse bending moment was 94791 kN·m, which appeared at 9.875 s in the initial period of the earthquake. The maximum vertical shear force was 3535 N, which appeared at 31.755 s. The structure's main force direction is a result of the main girder of a transverse earthquake.

3.1.2. Model 2 Seismic Response Analysis

The internal force responses of Model 2 under the three-way seismic input are listed in Table 5 to Table 7.

Table 5. Transverse seismic response of the bridge (force unit: kN, bending moment unit: kN·m)

Position	Internal force	Seismic Wave 1	Seismic Wave 2	Seismic Wave 3	Maximum value	Average value	Response Spectrum Results
Pier top	shear force *Fy*	2040	1739	2818	2818	2199	2673
	bending moment *Mx*	3178	2382	4368	4368	3309	3983
Pier bottom	shear force *Fy*	2169	1831	2947	2947	2316	3436
	bending moment *Mx*	19308	16200	24877	24877	20128	12342
Cantilever root	shear force *Fy*	1959	1656	2663	2663	2093	2185
	bending moment *Mz*	39007	37676	58488	58488	45057	32793

The transverse shear force and transverse bending moment at the top of the pier were lower than those at the bottom. In addition, the axial forces were both small. The calculation control parameter was the transverse bending moment at the bottom of the pier. The calculated results for the three seismic waves were relatively close, and their average seismic responses were close to the calculated results of the response spectrum. As shown in Table 6, under the longitudinal seismic input of the longitudinal bridge, the main response to the earthquake is the longitudinal bending moment of the bottom and top of the pier. Table 7 shows that under vertical seismic input, the main response of the earthquake is the

Table 6. Response of the longitudinal bridge seismic

Position	Internal force	Seismic Wave 1	Seismic Wave 2	Seismic Wave 3	Maximum value	Average value	Response Spectrum Results
Pier top	axial force *Fz*	5445	5785	5532	5785	5587	2615
	shear force *Fx*	4410	4820	4776	4820	4669	4101
	bending moment *My*	21700	23709	23462	23709	22957	21746
Pier bottom	axial force *Fz*	5449	5789	5535	5789	5591	2643
	shear force *Fx*	4562	4967	4954	4967	4828	3128
	bending moment *My*	23470	25596	25434	25596	24833	21405
Cantilever root	bending moment *My*	15139	16093	16163	16163	15798	18335

Table 7. Response of the vertical seismic

Position	Internal force	Seismic Wave 1	Seismic Wave 2	Seismic Wave 3	Maximum value	Average value	Response Spectrum Results
Pier top	axial force Fz	3145	2123	3912	3912	3060	5033
	shear force Fx	423	417	445	445	428	2038
	bending moment My	2484	2366	2960	2960	2603	5026
Pier bottom	axial force Fz	3237	2188	3915	3915	3113	2909
	shear force Fx	442	434	499	499	458	2058
	bending moment My	1880	1924	1953	1953	1919	4232
Cantilever root	shear force Fz	1770	1402	2157	2157	1776	2383
	bending moment My	16727	15487	23336	23336	18517	25377

longitudinal bending moment at the cantilever root of the main girder, and the longitudinal bending moment of the cantilever root exceeds the longitudinal seismic response of the longitudinal bridge. The above calculation results of the internal force time-history curve of each section were extracted and compared with the results of Model 1, as shown in Fig. 8.

The calculation results demonstrated that the seismic response of Model 1 at each control section was greater than that of Model 2. The bottom of the pier was consolidated in Model 1, and the cantilever end of the girder was the free end. Model 2 imposes vertical

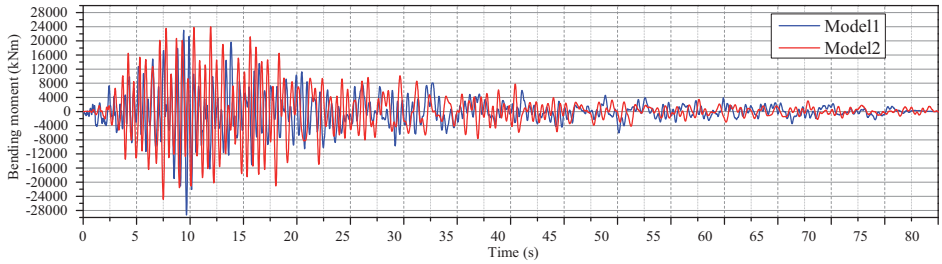

(a) Time history of bending moment (*Mx*)

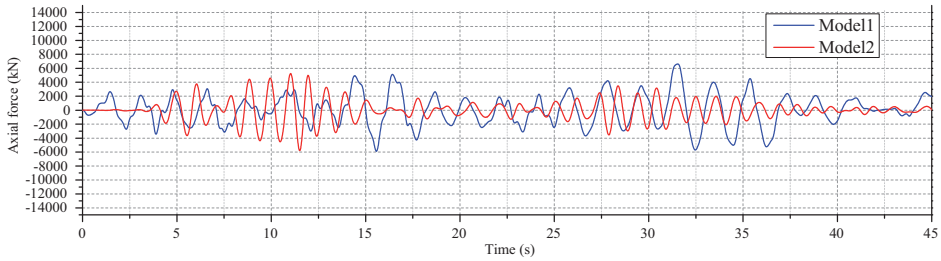

(b) Time history of axial force (*Fz*)

Fig. 8. Comparison of internal force response of pier bottom

and lateral horizontal constraints on the cantilever end of the girder through basin rubber bearings on both sides of the piers. Under lateral earthquake action, the lateral constraints of the side piers limit the lateral displacement of the structure, and they limit the lateral bending moment of the bridge together with the bottom constraints of the middle piers. This reduces the lateral bending moment response of the middle pier section, which is transformed into the lateral bending moment of the side. The maximum bending moment of the bottom section of the Model 2 pier was 24877 kN·m.The seismic response was reduced by 15%. The maximum axial force of the pier bottom section was 5789 kN, a 7% reduction; the maximum axial force of the pier top was 5785 kN, a 13% reduction, and the maximum bending moment value of the girder was 58488 kN·m, a 38% reduction. The side pier significantly reduced the bending moment response of the girder and the vertical seismic response of the middle pier through vertical restraint, which was transformed into the vertical axial force of the side pier. The middle pier resisted the external force in the longitudinal bridge direction, and the side pier's restraint capacity was limited. Therefore, the effects of the bending moments of the top and bottom sections of the middle pier were essentially the same under a longitudinal earthquake. The above analysis shows that the seismic response of the bridge under the maximum cantilever state is the core of the seismic calculation of the swivel structure. In addition to the girder's calculation and pier structure, the stress state of the spherical hinge and the support foot as a result of seismic action must be analyzed to determine whether it reaches the ultimate bearing capacity state or the structure suffers lateral instability.

This study adopted the finite element calculation method and used the maximum cantilever state as the research object. Furthermore, it selected a real seismic wave as the external excitation for time history analysis. Hence, the calculated results were close to the actual engineering situation. The time history analysis process involves a large number of iterations, with the total number of iterations for the two models exceeding 900,000. The calculation time is more than two days, which increases the time to complete the project. Moreover, this study proposes an optimization algorithm for the seismic response that shortens the calculation time of the time history analysis under the premise of obtaining a certain calculation accuracy based on the characteristics of the horizontal swivel system.

3.2. Optimization algorithm for seismic response of asymmetric continuous girder bridge horizontal swivel system

3.2.1. Proposition of Optimization Algorithms

The swivel structure can be simplified as an elastic system with multiple degrees of freedom. The seismic response calculation steps are as follows: First, the natural vibration period of the system is calculated to obtain $T_1, T_2, \ldots, T_n$, and the seismic is calculated to influence coefficients $\alpha_1, \alpha_2, \ldots, \alpha n$ under the natural vibration period. The mode shape participation coefficients are calculated to obtain $\gamma_1, \gamma_2, \ldots, \gamma_n$; furthermore, the seismic effect at each position is calculated using the formula $F_{ji} = \gamma_j x_{ji} \alpha_j G_i$; finally, the total effect of the earthquake can be obtained using the SRSS method.

Based on the vibration equation:

$$[M]\{x''(t)\} + [C]\{x'(t)\} + [k]\{x(t)\} = -[M]\{I\}x''(t) \tag{3.1}$$

where $[M]$ denotes the mass matrix, $[C]$ the damping matrix, $[k]$ denotes the stiffness matrix, $x(t)$ is the displacement function of the structure. The first and second derivatives represent the velocity and acceleration functions of the structure, respectively. The structural system has n mode shapes, and the mode shape matrix can be expressed as:

$$[A] = [\{x\}_1 \{x\}_2 \ldots \{x\}_n] \tag{3.2}$$

In the formula, the displacement matrix expression is $\{x(t)\} = [\{x\}_1 q_1(t) + \{x\}_2 q_2(t) + \ldots + \{x\}_n q_n(t)] = [A]\{q\}$, where $\{q\}$ is a coordinate vector in a broad sense. The displacement matrix is embedded into Eq. (3.1) to obtain the following formula:

$$M_j^* q_j'' + C_j^* q_j' + k_j^* q_j = -\{X\}_j^T [M]\{I\}x''(t) \tag{3.3}$$

In Eq. (3.3), $M_j^* = \{X\}_j^T [M]\{X\}_j^T$, $C_j^* = \{X\}_j^T [C]\{X\}_j^T$, $K_j^* = \{X\}_j^T [k]\{X\}_j^T$. The formula is changed, and the following is obtained:

$$q_j'' + 2\zeta_j \omega_j q_j' + \omega_j^2 q_j = -\gamma_j x''(t) \tag{3.4}$$

where γ_j is the mode shape participation coefficient, which is expressed as follows:

$$\gamma_j = \frac{\{X\}_j^T [M] \{I\}}{\{X\}_j^T [M] \{X\}_j} = \frac{\sum_{i=1}^{n} m_i x_{ji}}{\sum_{i=1}^{n} m_i {x_{ji}}^2} \tag{3.5}$$

The mass point i is subjected to a unit mass load of $x_{ji}\Delta_j(t)\gamma_j$, and is assigned by γ_j it to the j mode shape, as follows:

$$q_j(t) = -\frac{\gamma_j}{w_j} \int_0^t e^{-\rho_J w_j (t-\tau)} x_0''(\tau) \sin w_j(t-\tau) \mathrm{d}\tau = \Delta_j(t)\gamma_j \tag{3.6}$$

Then, the displacement of the j mode shape is $x_{ji}\Delta_j(t)\gamma_j$, and the displacement and acceleration expressions of all mode shapes are as follows:

$$x_i(t) = \sum_{j=1}^{n} \gamma_j \Delta_j(t)\gamma_j, \quad {x_i}''(t) = \sum_{j=1}^{n} \gamma_j {\Delta_j}''(t)\gamma_j \tag{3.7}$$

The expression of inertial force at particle$i$ in the structure must be:

$$F_i(t) = m_i \left[{x_i}''(t) + {x_0}''(t)\right] \tag{3.8}$$

According to the structural kinematics equation, the inertial force on particle i is:

$$F_{ji}(t) = m_i \left[\gamma_j {\Delta_j}''(t) x_{ji}(t) + \gamma_j x_{ji} {x_0}''(t)\right] \tag{3.9}$$

Then the maximum inertial force should be obtained through the following formula:

$$F_{(ji)\max} = m_i \gamma_j x_{ji} \left|\left[{\Delta_j}''(t) + {x_0}''(t)\right]\right| \tag{3.10}$$

In the formula: $\Delta_j''(t)$ is the seismic acceleration in the initial acceleration $x_0''(t)$ state. And $\left|\left[\Delta_j''(t) + x_0''(t)\right]\right|$ can be obtained from the response spectrum determined according to the seismic fortification intensity and the site characteristic period. Rewriting the above formula, the following formula is obtained:

$$F_{ij} = \gamma_j x_{ji} \alpha_j G_i \tag{3.11}$$

where α_j is the horizontal seismic influence coefficient $\alpha_j\left(T_j\right)$ of the j-th mode shape, x_{ji} is the horizontal relative displacement of the i particle position of the j-th mode shape, and γ_j is the j-th mode shape participation coefficient. According to the SRSS method, when the seismic action effect of all modes is considered, the following formula is used:

$$S = \sqrt{\sum S_j^2} \tag{3.12}$$

3.2.2. Example: Calculation of Seismic Effects during Rotation

The basic seismic acceleration of the horizontal swivel system was 0.1 g, the characteristic period of the site was 0.45 s, and the damping ratio of the structure was 0.05. The thrust stiffness of the bridge pier was $k_1 = k_2 = 3EI/H$, where E is the elastic modulus of the bridge pier, I is the transverse bending moment of inertia of the bridge pier, and H is the height between the bridge pier foundation and main girder. The motion of the rotating body structure was equivalent to the motion of an elastomer with two degrees of freedom. Mass point 1 was the position of the centroid of the pier, and mass was the mass of the pier itself, $m_1 = 686t$. Mass point 2 was at the top of the pier, and the mass was the total mass of the girder of the superstructure and second-stage dead load, $m_2 = t$. According to the kinematic equation, the following can be obtained.

$$\left(\begin{bmatrix} k_{11} & k_{12} \\ k_{21} & k_{22} \end{bmatrix} - \omega^2 \begin{bmatrix} m_1 & 0 \\ 0 & m_2 \end{bmatrix} \right) \begin{pmatrix} x_1 \\ x_2 \end{pmatrix} = \begin{pmatrix} 0 \\ 0 \end{pmatrix}$$

$k_{11} = k_1 + k_2$, $k_{12} = k_{21} = -k_2$, $k_{22} = k_2$, so:

$$\left| \begin{bmatrix} k_{11} & k_{12} \\ k_{21} & k_{22} \end{bmatrix} - \omega^2 \begin{bmatrix} m_1 & 0 \\ 0 & m_2 \end{bmatrix} \right| = 0$$

Combining the formulas obtains the following:

$$\left| \begin{bmatrix} k_{11} - \omega^2 m_1 & k_{12} \\ k_{21} & k_{22} - \omega^2 m_2 \end{bmatrix} \right| = 0$$

The angular frequency can be obtained from the above formula, and the mode-shape diagrams at different natural frequencies can be obtained by solving the displacement matrix. The transverse main vibration modes of the piers were determined and solved by calculating the first several vibration modes of the structure. Through the finite element analysis above, the first and seventh modes in Model 1 mode shape are the first- and second-order transverse bending mode shapes of the bridge pier, respectively. Furthermore, the results of the modal calculation are directly used in the calculation. The natural frequency of the seventh-order mode was 4.358 Hz. The period was 0.230 s, the natural frequency of the first-order mode was 4.06 Hz, and the period was 2.564 s. The seventh mode in the finite element model was considered as the first mode shape of the calculation, that is, $T_1 = 0.230$ s. The first mode was used as the second-mode shape for the calculation: $T_2 = 2.564$ s. The mode-shaped displacement is shown in Fig. 9. The natural vibration displacement was normalized to obtain the natural vibration law of the elastomer with two degrees of freedom.

Seismic action of the horizontal force of the first-order mode shape: According to the design response spectrum, the seismic acceleration of the horizontal earthquake was 0.1 g, and the influence coefficient of the horizontal earthquake was $\alpha_{\max} = 0.08$. Since $T_g = 0.45$ s, $0.1 < T_1 < T_g$, then $\alpha_1 = \alpha_{\max} = 0.08$. From (9), the following can be

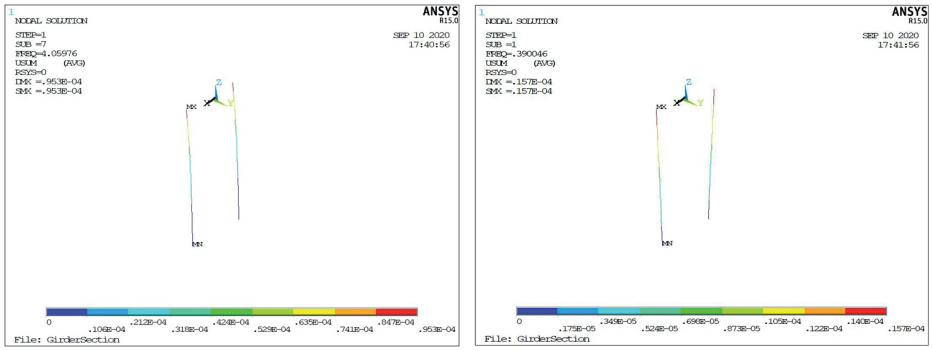

(a) (b)

Fig. 9. First and second order transverse bending modes of bridge piers

obtained:

$$\gamma_1 = \frac{\sum_{i=1}^{n} m_i x_{ji}}{\sum_{i=1}^{n} m_i x_{ji}^2} = \frac{1.0 \times 686 + 2.1 \times 11348}{1.0^2 \times 686 + 2.1^2 \times 11398} = 0.483$$

Substituting the above equation into Equation (3.12), we obtained the horizontal seismic force on the two mass points:

$F_{11} = \gamma_1 x_{11} \alpha_1 G_1 = 0.483 \times 1.0 \times 0.08 \times 686 \times 10 = 265.1$ kN

$F_{12} = \gamma_1 x_{12} \alpha_1 G_2 = 0.483 \times 2.1 \times 0.08 \times 11398 \times 10 = 9248.8$ kN

Similarly, the horizontal seismic action of the second mode shape can be obtained as $T_2 > 5T_g$, according to the design response spectrum, $\alpha_2 = 0.037$.

$$\gamma_2 = \frac{\sum_{i=1}^{n} m_i x_{ji}}{\sum_{i=1}^{n} m_i x_{ji}^2} = \frac{1.0 \times 686 + 1.7 \times 11398}{1.0^2 \times 686 + 1.7^2 \times 11398} = 0.60$$

then horizontal seismic force should be:

$F_{21} = \gamma_1 x_{11} \alpha_1 G_1 = 0.6 \times 1.0 \times 0.014 \times 686 \times 10 = 58$ kN

$F_{22} = \gamma_1 x_{12} \alpha_1 G_2 = 0.6 \times 1.7 \times 0.014 \times 11398 \times 10 = 1628$ kN

According to the SRSS method, after the two mode shapes were superimposed, $F_1 = 271$ kN and $F_2 = 9391$ kN, and the bending moment of the pier bottom $Mx' = 271(10 - 2.9)/2 + 9391(10 - 2.9) = 67638$ kN·m. The finite element result is $Mx = 229296 = 58592$ kN·m, and the optimization algorithm was 87% of the finite element calculation result, which is close to the finite element calculation result.

4. Conclusions

In this study, the mechanical behavior of an asymmetric continuous girder bridge horizontal swivel system under earthquake action was studied, and the following conclusions were reached:

First, this study is based on the seismic data of the Pacific Earthquake Engineering Research Center (PEER) and screens out six seismic waves of Models 1 and 2 in three directions that meet the calculation requirements. The calculated results for actual seismic waves are relatively discrete. However, the average value is close to the response spectrum method's calculated results.

Second, the main seismic responses of Model 1 were the lateral bending and vertical axial force of the pier bottom, as well as the longitudinal and lateral bending of the main girder. In Model 2, the lateral bending moment and vertical axial force at the bottom of the pier were reduced by 15% and 7%, respectively. Furthermore, the maximum bending moment of the main beam at the cantilever root was reduced by 38%. The side piers bear a part of the internal force of the middle piers, and the seismic design of the asymmetric continuous girder's bridge horizontal swivel system focuses on main beam stress analysis during the translation process.

Third, based on the mode shape superposition method, an optimization algorithm for the seismic response of a horizontal swivel system of asymmetric continuous girder bridges was proposed. The results of the optimization algorithm indicate high accuracy, 87% of the finite element.

Acknowledgements

This work is supported by four projects: (1) Research on the influence of ultra-high performance concrete strengthened RC beams based on oriented fiber arrangement on shear performance, Natural science research project of universities in Anhui Province, and the project number is KJ2021A0504. (2) Research on Mechanical Characteristics and Design Method of hoop constraint UHPC Spherical Hinge in Bridge Swivel, Pre research project of National Natural Science Foundation of Anhui Polytechnic University, and the project number is Xjky2022173. (3) Study on mechanical characteristics and design method of ultra-high performance concrete spherical hinge translational system under multi factor coupling, The Initial Scientific Research Funds of Anhui polytechnic University", and the project number is 2021YQQ021. (4) Experimental study on properties of metal slag concrete mixed with glass fiber, Scientific research project of Anhui University of Engineering, and the project number is Xjky110201909.

References

[1] T. Siwowski and A. Wysocki, "Horizontal rotation via floatation as an accelerated bridge construction for long-span footbridge erection: Case study", *Journal of Bridge Engineering*, vol. 20, no. 4, pp. 124–126, 2015, DOI: 10.1061/(ASCE)BE.1943-5592.0000693.

[2] J.W. Wang, B. Cao, and B. Huang, "Stability monitoring method of UHPC spherical hinge horizontal rotation system", *Archives of Civil Engineering*, vol. 68, no. 3, pp. 601–616, 2022, DOI: 10.24425/ace.2022.141905.

[3] J. Du, "Innovation and Prospect of bridge Swivel Construction Technology", *Railway Construction Technology*, vol. 2012, no. 4, pp. 7–11, 2012.

[4] D.R. Gharpure and R.B. Sachin, "Poira bridge: Construction of India's first horizontal swing bridge", *Indian Concrete Journal*, vol. 81, no. 8, pp. 33–35, 2007.

[5] J. Zhang, T.E. El-Diraby, "Constructability analysis of the bridge superstructure rotation construction method in China", *Journal of Construction Engineering and Management*, vol. 132, no. 4, pp. 353–360, 2006, DOI: 10.1061/(ASCE)0733-9364(2006)132:4(353).

[6] T. Siwowski and A. Wysocki, "Horizontal rotation via floatation as an accelerated bridge construction for long-span footbridge erection: Case study", *Journal of Bridge Engineering*, vol. 20, no. 4, pp. 124–126, 2015, DOI: 10.1061/(ASCE)BE.1943-5592.0000693.

[7] E. Watanabe, T. Maruyama, H. Tanaka, and S. Takeda, "Design and construction of a floating swing bridge in Osaka", *Marine Structures*, vol. 13, no. 4-5, pp. 437–445, 2000, DOI: 10.1016/S0951-8339(00)00016-2.

[8] C. Wang, "Integral stress analysis and pier optimization design of T-shaped rigid frame bridge with Swivel Construction", M.A. thesis, Southwest Jiaotong University, 2017.

[9] X. Wang, "Numerical analysis of ANSYS engineering structure", *Bei Jing: People's Communications Press*, pp.10-49, 2007.

[10] S. Huang, "National standards of the people's Republic of China: Code for seismic design of buildings (GB 50011-2010)", China Construction Industry Press, 2016.

[11] Y. Tang, "National standards of the people's Republic of China: Detailed rules for earthquake resistance of Highway Bridges (GBT50152-2012) [S]", People's Communications Press, 2012.

Received: 2022-11-21, Revised: 2022-12-13